Efficient removal of anionic Amaranth azo dye from the aqueous environment using papaya leaf stalks: Studies on batch adsorption, mechanism, and desorption

Venkata Subbaiah Munagapati, Hsin-Yu Wen, Anjani R. K Gollakota, Jet-Chau Wen, Kun-Yi Andrew Lin, Chi-Min Shu, Vijaya Yarramuthi, Praveen Kumar Basivi, Chang Woo Kim & Jeung-Tai Tang

Published online: 08 Dec 2024.

Submit your article to this journal 🗗

View related articles 🗗

View Crossmark data 🗗

Taylor & Francis
Taylor & Francis Group

Check for updates

Efficient removal of anionic Amaranth azo dye from the aqueous environment using papaya leaf stalks: Studies on batch adsorption, mechanism, and desorption

Venkata Subbaiah Munagapati[a], Hsin-Yu Wen[b], Anjani R. K Gollakota[c], Jet-Chau Wen[a,d], Kun-Yi Andrew Lin[e,f], Chi-Min Shu[d], Vijaya Yarramuthi[g], Praveen Kumar Basivi[h], Chang Woo Kim[i], and Jeung-Tai Tang[j]

[a]Research Centre for Soil & Water Resources and Natural Disaster Prevention (SWAN), National Yunlin University of Science and Technology, Douliou, Yunlin, Taiwan; [b]Department of Pathology, West China Hospital, Sichuan University, Chengdu, PR China; [c]Department of Chemical and Materials Engineering, National Yunlin University of Science and Technology, Douliou, Yunlin, Taiwan; [d]Department of Safety, Health, and Environmental Engineering, National Yunlin University of Science and Technology, Douliou, Yunlin, Taiwan; [e]Department of Environmental Engineering & Innovation and Development Center of Sustainable Agriculture, National Chung Hsing University, Taichung, Taiwan; [f]Institute of Analytical and Environmental Sciences, National Tsing Hua University, Hsinchu, Taiwan; [g]Department of Chemistry, Vikrama Simhapuri University, Nellore, Andhra Pradesh, India; [h]Pukyong National University Industry-University Cooperation Foundation, Pukyong National University, Busan, Republic of Korea; [i]Department of Nanotechnology Engineering, College of Engineering, Pukyong National University, Busan, Republic of Korea; [j]Department of Information & Management, National Yunlin University of Science and Technology, Douliou, Yunlin, Taiwan

ABSTRACT

Papaya leaf stalks (PLS) were utilized in the current research to eliminate Amaranth (AM) dye from an aqueous medium. PLS was characterized through various techniques, including BET/BJH, pH_{PZC}, XRD, FTIR, FESEM, and EDX. The FTIR analysis unveiled that -OH (hydroxyl), -C=O (carbonyl), and -COOH (carboxylic) groups were involved in binding AM to the surface of PLS. Batch mode adsorption tests were conducted, and various operational variables like pH, the mass of PLS, AM dye concentration, contact duration, stirring speed, temperature, and regeneration of the PLS were investigated. The maximal AM removal efficiency of $91.1 \pm 2.601\%$ was observed at pH 2.0. The pH_{PZC} of the PLS was determined to be 5.5. The experiment results were analyzed using isotherm models (Freundlich, Temkin and Langmuir) and kinetic models (pseudo-second-order and pseudo-first-order). The pseudo-second-order kinetic and Langmuir isotherm models provided the best fit. The maximal sorption uptake of AM dye on PLS was achieved at 121.3 ± 1.493 mg/g at 298 K. The thermodynamic variables indicated that the sorption process was spontaneous ($\Delta G^o < 0$), exothermic ($\Delta H^o > 0$), and feasible ($\Delta S^o > 0$) at different temperatures. The AM adsorption on PLS was mainly due to electrostatic interactions. Desorption tests were also carried out to investigate the feasibility of regenerating PLS, and $89.2 \pm 1.184\%$ of the adsorbed AM was recovered using 0.2 M-NaOH. The reusability results indicated that $76.9 \pm 2.204\%$ of the adsorption efficiency could still be maintained even after six cycles. These results demonstrate that PLS is an environmentally friendly and suitable material for removing AM from wastewater.
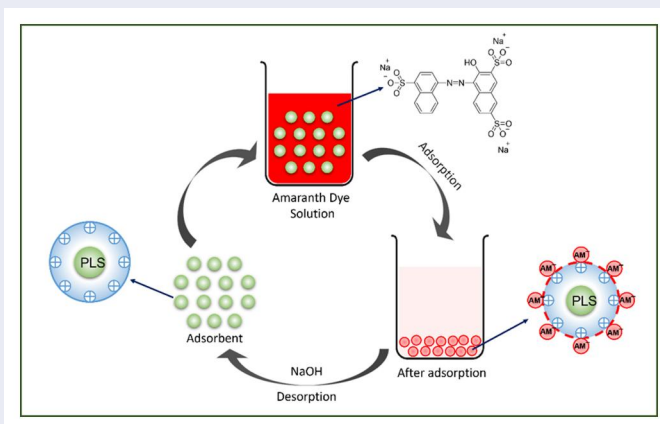
GRAPHICAL ABSTRACT

CONTACT Jet-Chau Wen ✉ wenjc@yuntech.edu.tw ▣ Research Centre for Soil & Water Resources and Natural Disaster Prevention (SWAN), National Yunlin University of Science and Technology, Douliou, Yunlin 64002, Taiwan; Kun-Yi Andrew Lin ✉ linky@nchu.edu.tw ▣ Department of Environmental Engineering & Innovation and Development Center of Sustainable Agriculture, National Chung Hsing University, Taichung, Taiwan.

1. Introduction

In recent years, the global focus has shifted toward sustainable development policies, prompted by the rapid advancement of industrial technology and the diminishing availability of natural resources. Notably, the pollution of water resources by various countries has become a central concern. Synthetic dyes play a pervasive role across diverse industries, including textiles, leather, cosmetics, pharmaceuticals, petrochemicals, and others, with a worldwide annual production and utilization rate of approximately 700,000 metric tons.[1] Among the hazardous water pollutants, synthetic dyes stand out, containing components that pose toxicity, carcinogenicity, teratogenicity, or mutagenicity risks to aquatic organisms and humans.[2]

Amaranth (AM), a dark red water-soluble synthetic dye extensively used in the beverage and food industry, also serves as a coloring agent in phenol-formaldehyde resins, wood, textiles, leather, and paper. However, during these processes, some excess dye gets into the water.[3,4] If this dye-laden wastewater is not treated before being discharged into surface waters, it can significantly affect the water's transparency and esthetics. Furthermore, they may impede sunlight and oxygen penetration, posing harm to aquatic life.[5] Additionally, AM dye is associated with various adverse health effects, including mutagenicity, birth defects, allergies, cytotoxicity, respiratory problems, carcinogenicity, genotoxicity, and tumors.[6] Therefore, it is vital to eliminate AM dye from wastewater before it is discharged into the environment by employing a proper treatment method.

Many treatment technologies, including ultrafiltration, ion exchange, photocatalysis, oxidation, and biological degradation, have been applied to eliminate dyestuffs from wastewater.[7] However, these methods encounter challenges such as non-scalability, intricate operations, high generation of secondary chemical waste, and elevated removal costs. Consequently, there is a pressing need for the development of technologies that are efficient, cost-effective, low-energy consuming, and generate minimal secondary waste. In light of this, adsorption has emerged as a promising approach. Intensive efforts have been directed toward identifying efficient adsorbents for removing dyes from contaminated water.

While activated carbon derived from coal has proven effective as an adsorbent for dye removal, its widespread application is hindered by high production costs.[8] Consequently, the development of low-cost bio-based biosorbents becomes imperative for practical applications. Careful consideration is essential in selecting adsorbents, as achieving a delicate balance is crucial in developing bio-based materials. This balance should encompass factors such as adsorption efficiency, development costs, practical applicability, and the final disposal process after biosorption. Many sorbent materials obtained from natural resources like banana peel,[9] manila tamarind seed powder,[10] citrus limetta peel,[11] papaya bark fiber,[12] sugarcane bagasse,[13] litchi leaves powder,[14] corn stalks,[15] eucalyptus angophoroides bark,[16] avocado seed powder,[17] etc have been used for removing dyes from wastewater.

Modifying and functionalizing the surfaces of adsorbents derived from biomass is crucial for increasing their adsorption uptake and selectivity. Altering the surface through processes such as activation, functionalization, and impregnation with specific reagents or chemicals introduces new functional groups and enhances the number of sorption sites. This results in improved selective sorption behavior based on the incorporated functional groups. Introducing charged moieties on the surface leads to selective behavior, allowing the targeting of pollutants with opposite charges. These modifications are attributed to an increase in adsorption sites and the addition of functional groups, which in turn enhances the efficiency of the adsorbent in mitigating contaminants. Various factors influence adsorption uptake, including size and charge of the adsorbate, surface area, porous structure, surface chemistry (functional groups), and interactions between the adsorbent and adsorbate.[18] Various waste biomaterials, including cationic amino-modified walnut shell,[19] acid treated lathyrus sativus husk,[20] base modified artocarpus odoratissimus leaves,[21] pine cone powder modified with β-cyclodextrin,[22] activated carbon from peanut shell,[23] etc., have been studied as adsorbents to remove dyes from wastewater. However, in some cases, the intrinsic properties of unaltered materials can yield better results than modified ones, especially regarding costs, environmental effects, biodegradability, non-toxicity, renewable nature, and the specific requirements of the required adsorption process.

The fruit-bearing plant papaya, scientifically known as *Carica papaya*, is native to Central and South America. Now this is cultivated in numerous tropical and subtropical regions globally. It is a compact, rapidly growing tree with the potential to reach heights of up to 10 meters, although it typically remains shorter. The leaves are characterized by large size and deep lobes and the trunk is soft and sappy. Papaya leaf stalks (PLS) refer to the slender, elongated stems linking the papaya leaves to the tree's main trunk. Despite often being disregarded, these leaf stalks contain beneficial compounds and can serve various purposes. In traditional medicine, PLS is sometimes utilized to address various health issues, including fever, malaria, and dengue fever. The PLS is a fibrous material that contains various functional groups like amine, hydroxyl, carbonyl, and carboxyl groups. PLS are also rich in cellulose, hemicellulose, and lignin, which are all complex organic compounds that can aid in the adsorption of pollutants in wastewater. The PLS's fibrous structure and high surface area allow them to adsorb pollutants and contaminants from the wastewater effectively. No studies have been reported on the PLS as an adsorbent for AM dye removal.

The objectives of this study were to evaluate the feasibility of using PLS to eliminate AM from aqueous media. Various characterization techniques, such as BJH/BET, XRD, pH$_{PZC}$, FTIR, EDX, and FE/SEM, were employed to comprehensively analyze the surface characteristics of PLS before and after adsorption. The effects of different process variables, including pH, PLS dose, initial AM dye concentration, contact duration, and temperature, on adsorption were

investigated, and conditions were optimized. The pseudo-second and first-order kinetic models were used for the analysis of the kinetic adsorption data. The Temkin, Freundlich, and Langmuir isotherm models described the equilibrium data. Thermodynamic variables, including enthalpy, Gibbs free energy, and entropy, were evaluated based on the results at various temperatures. Additionally, the reusability of PLS was tested. The adsorption mechanism of AM dye uptake onto PLS was discussed.

2. Materials and methods

2.1. Reagents and chemicals

Sodium hydroxide (NaOH) and hydrochloric (HCl) acid were purchased from Merck (Germany), and Amaranth (AM) dye was obtained from Sigma-Aldrich (USA). Table 1 displays the structure of the AM dye and its key chemical properties. Each chemical was employed as a foundation and was of the quality of an analytical reagent. All the compounds were dissolved in an aqueous solution made using deionized (DI) water that had been prepared in the laboratory.
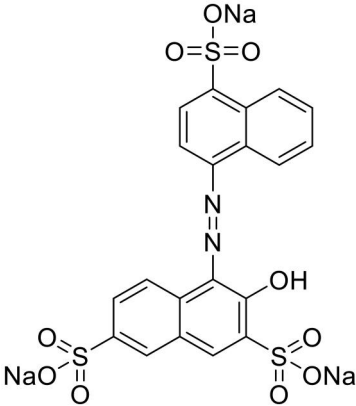
2.2. PLS preparation

Locally sourced papaya leaf stalks (PLS) were wholly cleaned with DI water to eliminate impurities and dirt. The stalks were then sliced into small pieces and dried in an oven at 80 °C for 24 h. After drying, the PLS was permitted to cool at room temperature and then crushed in a mixer grinder before being sifted through a 35-mesh sieve tray. Lastly, the prepared adsorbent was stored in an air-tight polythene bag.

2.3. Characterization

Field Emission-Scanning Electron Microscope (FE/SEM, JEOL, JSM-7610F, Japan) evaluated the surface morphology of the PLS before and after sorption. This was applied in conjunction with Energy Dispersive X-ray (EDX, UK,

Oxford Instruments) analysis to get data on the elemental composition. Before scanning, the materials were coated with gold to improve electron conductivity. The micrographs were examined at 500x magnification. Fourier Transform Infrared (FTIR, Thermo Fisher, Nicolet iS10, USA) instrument was used to characterize the functional groups of PLS before and after sorption at the wavelength range of 4000 to 400 cm^{-1}. A KBr pellet has been used for FTIR measurement, which is prepared by mixing the samples with IR grade KBr in the ratio of 1:100 by weight. The crystalline nature of PLS was examined using an X-ray Diffractometer (XRD, Advance Bruker D8, Germany) using CuKα radiation ($\lambda = 1.5417$ Å) associated with Kβ filter at room temperature at a voltage of 30 kV and 30 mA. The material was scanned at a rate of 5° per minute to obtain XRD structural data. The radiation intensity was plotted against 2θ ranging from 10 to 80°. The pore volume, surface area, and pore radius of the PLS were measured by conducting N$_2$ adsorption-desorption isotherm with Brunauer Emmett Teller (BET) and Barrett Joyner Halenda (BJH) methods by employing a Quantachrome Autosorb-iQ analyzer (USA). Before the analysis, sample degassing was done at 100 °C for 4–6 h. A UV Vis spectroscopy (JSACO, V750, Japan) was utilized to determine the residual dye concentration. The solid addition method determined the PLS's point of zero charges (pH$_{PZC}$). In this experiment, solutions with different pH values (2.0 to 11.0 ranging) were prepared by adding 0.1 M NaCl (30 mL each). The pH mediums were then adjusted using 0.1 M-HCl and 0.1 M-NaOH. After that, 50.0 mg of the PLS was added to each solution, and the mixture was agitated at 25 °C for 24 h. Following this, the suspension was filtered to separate the PLS and the final pH of the supernatant solution was determined using a digital pH meter (A214 Thermo Orion Star, USA). The variation between the initial and final pH values (ΔpH = final - initial) was calculated, and a plot was made by plotting ΔpH versus the pH initial values. The pH$_{PZC}$ value was obtained from the plot by identifying the point where the curve intersects the X-axis, indicating that the ΔpH is 0.

Table 1. Structure and physiochemical characteristics of AM dye.

Structure	
IUPAC name	Trisodium (4Z)-3-oxo-4-[(4-sulfonato-1-naphthyl)hydrozono]-3,4-dihydro-2,7-naphthalenedisulfonate
Nature	Anionic
Chemical formula	$C_{20}H_{11}N_2Na_3O_{10}S_3$
Molecular weight	604.473 g/mol
λ_{max}	520 nm

2.4. Adsorption and desorption experiments

Amaranth (AM) dye adsorption tests under various conditions were carried out, such as shaking time (50–400 min), pH solution (2.0–11.0), initial AM concentration (20–200 m/L), the dose of PLS (10–80 mg), and temperatures (298–328 K). In each test, a known amount of PLS was added to 30 mL of dye solutions and was kept in polypropylene tubes. The pH of the dye solution was adjusted using 0.1 M solutions of HCl/NaOH. The reaction mixtures were placed in a shaker under constant agitation. The collection of samples occurred at designated time intervals, and the adsorbents were separated by centrifugation at 3000 rpm for 10 min. The concentration of unadsorbed AM dye was subsequently ascertained using a UV/Vis spectrophotometer. The batch sorption tests were conducted multiple times, and the average values were used for data analysis. Finally, the removal (R%) and adsorption capacity (q_e) of AM dye over the PLS were estimated by the following equations:

$$R\% = \left(\frac{C_o - C_e}{C_o}\right) \times 100 \qquad (1)$$

$$q_e = \frac{(C_o - C_e)V}{M} \qquad (2)$$

where q_e (mg/g) signifies the quantity of adsorbate removed by a PLM at equilibrium, C_o and C_e (mg/L) is the primary and final AM concentration, M (g) is the PLS mass, and V (L) is the volume of AM solution.

The spent PLS was separated from the solutions after adsorption, and cleaned with DI water to remove any unadsorbed AM dye. Next, the samples were dried at 80 °C in an oven and added into a polypropylene tube containing 30 mL of different concentrations of NaOH (0.2 M to 1.0 M). This was done for the purpose of desorbing the AM. The tubes were kept in the shaker at the same temperature for the same duration as the adsorption experiments. After desorption, the AM dye desorbed (C_{de}) concentrations were measured using UV Vis spectrophotometry. The AM dye-desorbed PLS would subsequently be used for the next adsorption/desorption experiment cycle to evaluate its regeneration ability. To calculate the percentage of desorption, use the following equation.

$$desorption\ rate\ (\%) = \frac{AM_{de}}{AM_{ad}} \times 100 \qquad (3)$$

3. Results and discussion

3.1. Characterization of the PLS

FTIR analysis is typically utilized to identify the various functional groups on the sorbent material's surface. The FT-IR spectrum of PLS before and after the adsorption of AM on it is presented in Figure 1. In the spectra of PLS (Figure 1a), the broad peak was observed at around 3286 cm^{-1}, corresponding to phenolic/alcoholic O-H stretching vibration in the hydrogen-bonded form.[24] In lignin, hemicellulose, cellulose, and generally in aliphatic acids, the bands at 2922 and 2851 cm^{-1} correspond to asymmetrical and symmetrical C-H stretching
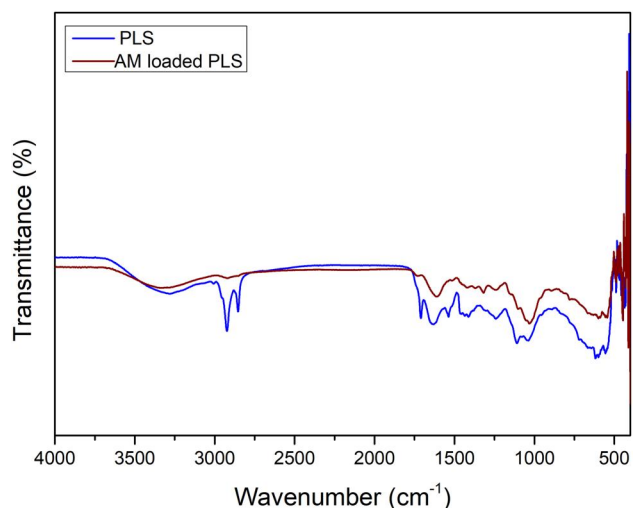

Figure 1. Comparative FTIR spectra of PLS before and after adsorption of AM dye.

of methoxyl groups.[25] The peak at 1710 cm^{-1} was assigned for the C=O bending vibrations in the carboxylic acid (-COOH) groups.[26] The stretching vibrations observed at 1632 cm^{-1} correspond to the structure's C=O groups (ketones, aldehydes, or carboxyl groups).[27] The 1537 cm^{-1} band corresponds to C=C stretching vibrations from lignin's aromatic rings.[28] The peak at 1409 cm^{-1} indicates asymmetric and symmetric stretching vibration in the ionic carboxylic group.[29] The peak at 1241 cm^{-1} displayed the existence of the phenolic OH or OH deformation of COOH.[30] The 1109 and 1036 cm^{-1} bands correspond to the C-O stretching vibration of carboxylic acids and alcoholic groups.[31] The band at 615 cm^{-1} is related to cellulose's strong C-H bending vibration. The surface of natural biomass often contains several functional groups, including residual –OH, -NH$_2$, and –COOH groups. After AM dye adsorption (Figure 1b), some bands are shifted (3286, 1710, 1632, 1409, 1241, 1036, and 615 cm^{-1} shifted to 3326, 1732, 1603, 1423, 1235, 1026, and 596 cm^{-1}) and some peaks are disappeared (2922, 2851, 1537, and 1109 cm^{-1}), indicating these functional groups participated in the AM adsorption of the surface of PLS through strong electrostatic interaction forces.

Figure 2 illustrates PLS's morphology and elemental composition before and after AM adsorption. As shown in Figure 2a, the outer surface of the PLS is porous, with rough borders, irregularities, and a heterogeneous structure. Surface roughness is essential in dye ion binding because it raises the surface area, facilitating dye sorption on the surface. After adsorption (Figure 2b), the surface of the PLS was entirely filled by the AM dye molecules, and the rough surface became smoother, indicating the successful attachment of AM molecules to the PLS surface. The EDX spectrum of the PLS shows the peaks of C, O, and Ca elements (Figure 2c). After adsorption, additional Na, Mg, Cl, K, and S peaks appeared in the spectrum of AM-PLS (Figure 2d); these peaks confirm that the AM dye molecules were loaded successfully onto the PLS surface.

PLS's adsorption/desorption isotherm was obtained at 77.0 K to determine the material's surface characteristics. The graph in Figure 3a illustrates the H$_3$ hysteresis loop and type-IV isotherm, which are classified by IUPAC based on
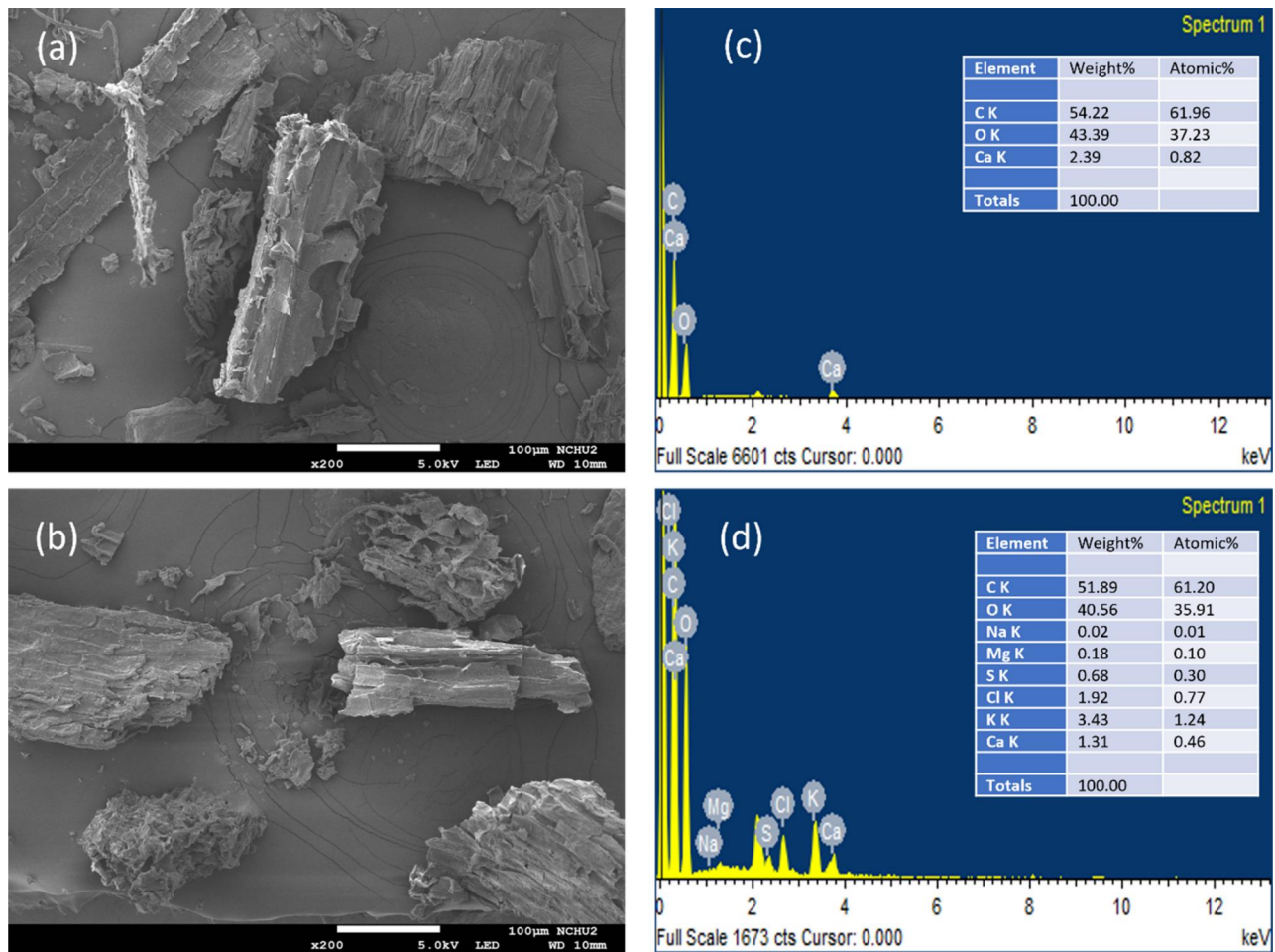
Figure 2. FE-SEM images of (a) PLS and (b) AM-loaded PLS; EDX images of (c) PLS and (d) AM-loaded PLS.
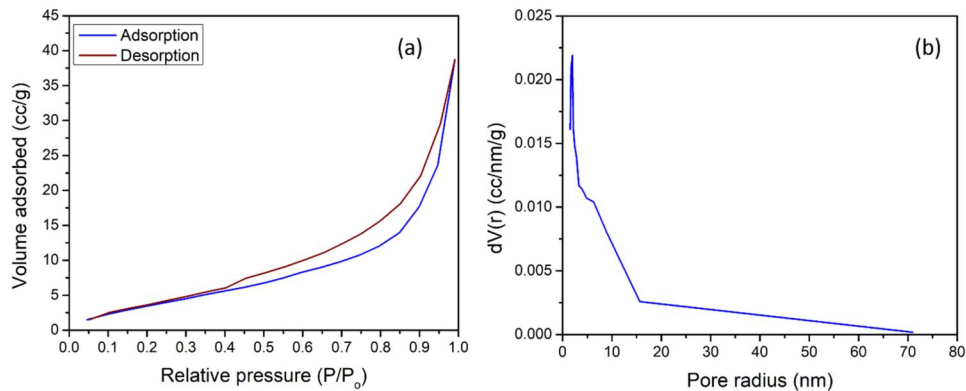

Figure 3. (a) N_2 adsorption-desorption isotherm and (b) pore size distribution of PLS.

the solid material's porosity. The H_3-type loop implies the existence of mesopores at P/P_o greater than 0.46, attributed to capillary condensation within the pores. The beginning segment (up to $0.46\,P/P_o$) of the type-IV isotherm corresponds to monolayer N_2 sorption and is akin to the beginning of the type-II isotherm. The next segment of the type-IV isotherm indicates multilayer sorption. Using the BET/BJH method, the results for surface area, pore radius, and pore volume were $16.24\,m^2/g$, $2.3\,nm$, and $0.1429\,cc/g$, respectively. The PLS's pore size distribution, as shown in Figure 3b, is around $2.3\,nm$, and the majority of its pores correlate to the IUPAC

classification's pore size, indicating that the material has mesoporous characteristics. Because of the mesoporous structure's large pore volume and surface area, AM was effectively adsorbed from wastewater in the PLS.

XRD analysis examined the as-prepared PLS for its crystalline or amorphous nature. The XRD pattern of PLS (Figure 4) showed an amorphous nature, which is attributed to its high content of organic compounds. The pattern showed two broad diffraction peaks at 2θ (degree) = $15.1°$ and $22.2°$, indicating the presence of hydroxyl, aldehyde, amine, and ketones moieties of hemicelluloses and cellulose in PLS.[32]

3.2. Influence of pH

The pH of the solution is vital during the sorption process because it might affect the charge and structure of the sorbents. It can impact the solubility of solutes in a liquid medium and the dissociation of functional groups found on the binding sites of biosorbents. The removal effectiveness of AM by PLS throughout a pH range of 2.0–11 is depicted in Figure 5a. Based on the data displayed in Figure 5a, it can be inferred that pH changes have notable impacts and provide unique insights into the interactions between adsorbate and adsorbent molecules. At pH 2.0, the highest removal of AM dye ($91.1 \pm 2.601\%$) was attained; however, as pH rises from 2.0 to 11.0, the percentage of dye removed continuously decreases, reaching a maximum of $5.2 \pm 1.716\%$. As a result, the pH value at which the net charge on the sorbent surface is zero is used to characterize the pH_{PZC} or point of zero charge. The intersection point shows the pH_{PZC} in the initial pH against the final pH plot, which is located at 5.5, according to Figure 5b. More protonated H^+ ions are present at pH levels lower than pH_{PZC}, which adds more positive charges to the PLS surfaces. The negatively charged anionic AM dye is more strongly attracted to the positive charges on the PLS surface, where it is bound by electrostatic contact forces. In general, physisorption is driven by electrostatic interactions between
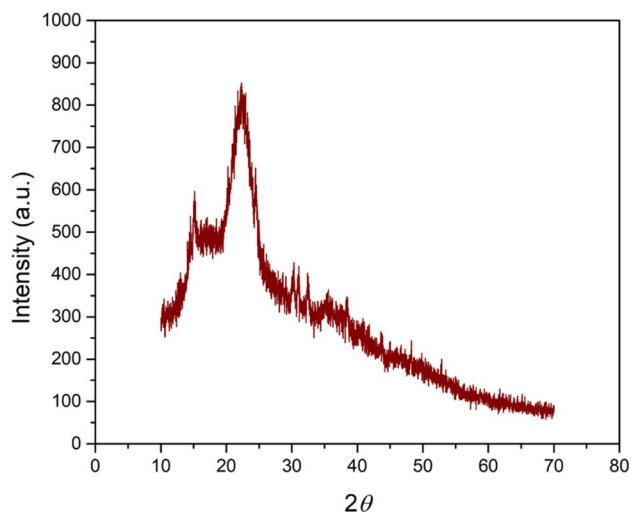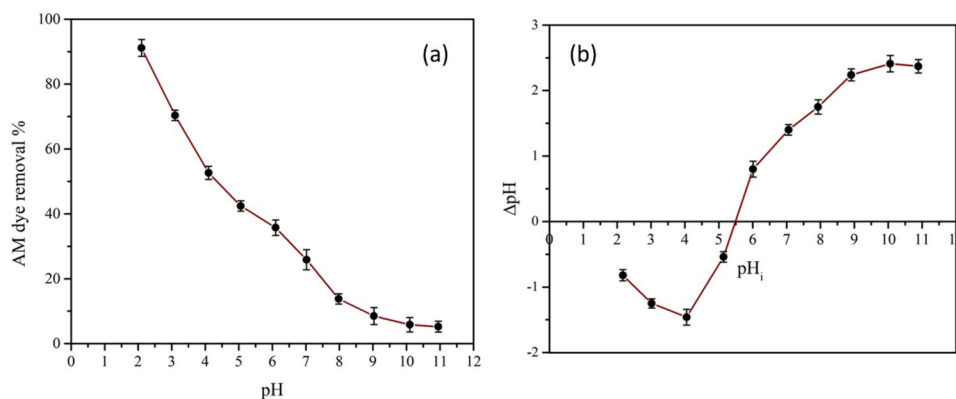
oppositely charged adsorbents and adsorbates; however, charged ions may interact *via* chemical bonds for chemisorption. AM adsorption on the PLS surface occurs only when the pH is lower than the pH_{PZC}, indicating that physisorption influences the sorption process. On the other hand, when the pH exceeds pH_{PZC}, the particle's surface becomes negatively charged, and the -OH ion that is already present in the solution competes with the arriving negatively charged anionic AM dye for the sorption sites. As a result, PLS's adsorption capabilities decrease when pH rises. Previous studies[2,33,34] have shown similar findings when investigating the removal of AM dye. Based on these results, a pH value 2.0 was chosen as the optimal condition for subsequent adsorption tests.

3.3. Impact of initial AM dye concentration

The efficiency of the biosorbent may be found by varying the pollutant solution's initially concentration. By doing this, the pushing force required to lower the barrier to mass transfer between the solid and liquid phases is created. Figure 6a illustrates the removal of AM dye at varying initial concentrations. The efficiency of AM dye removal decreased from 91.7 ± 1.326 to $54.2 \pm 1.142\%$ as the starting concentration of AM dye rose from 20.0 to 200 mg/L, respectively. This decrease can be linked to a dynamic balance between the dye molecules that are adsorbed and those that remain free in the solution. Nevertheless, when the concentration exceeds a specific threshold, there will be no active sites available for the dye molecules, as the adsorbent becomes saturated with them.[35] In this study, 20 mg/L was found to be the optimal initial concentration for efficient removal of AM dye due to its maximum removal efficiency.

3.4. Impact of stirring speed

The experiment was conducted to examine the effect of stirring speed on dye removal efficiency in the range of 50–400 rpm. The results of the study, presented in Figure 6b, show that dye removal efficiency increased from $36.5 \pm 1.551\%$ to $91.9 \pm 1.625\%$ as the agitation speed rose from 50 to 250 rpm. After 250 rpm, the efficiency remained constant. The raised efficiency can be attributed to the high
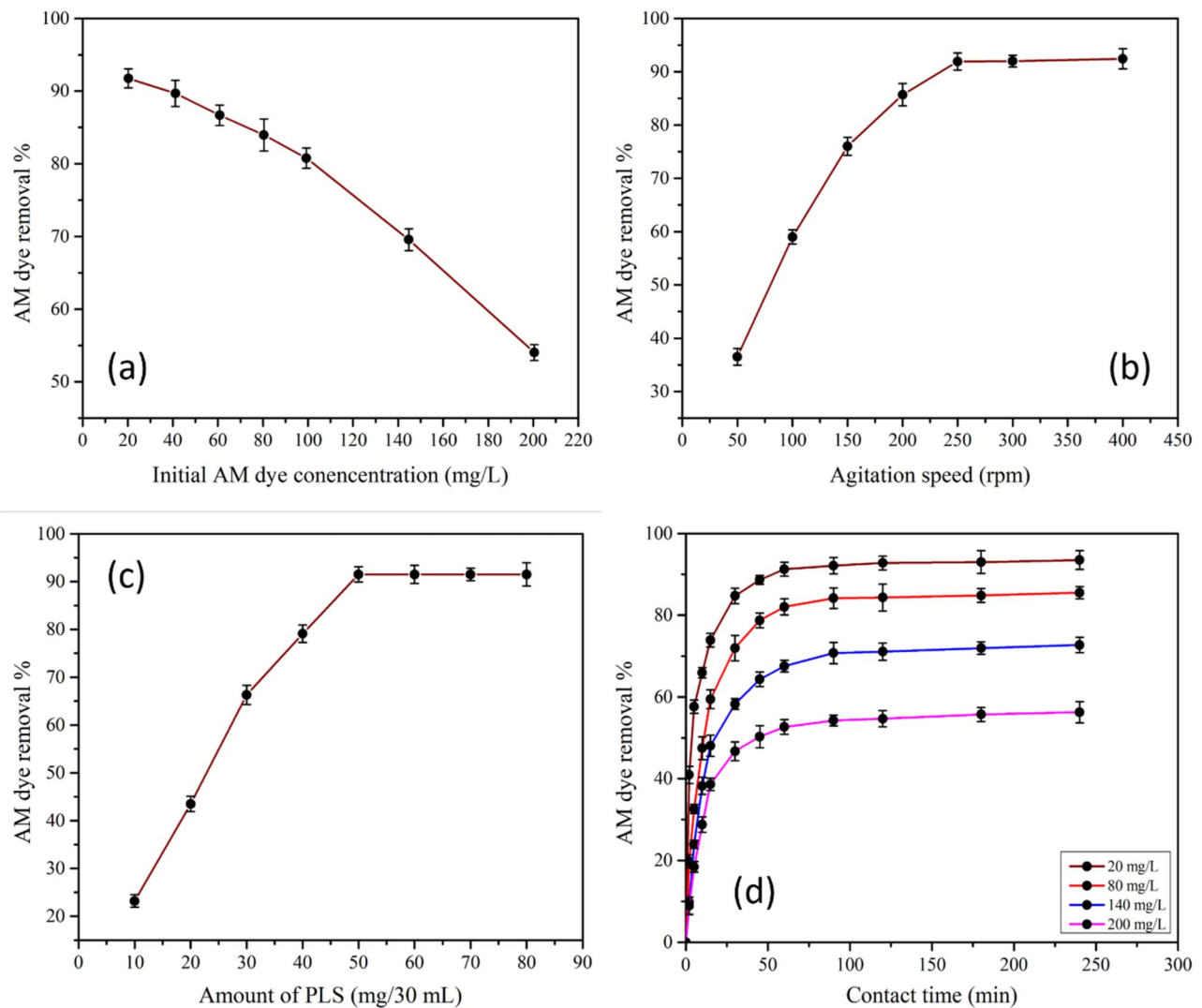

Figure 4. XRD pattern of PLS.

Figure 5. (a) Effect of pH on the % removal of AM by PLS and (b) pH at point of zero charge of PLS.

Figure 6. Effect of parameters, (a) initial AM concentration, (b) agitation speed, (c) amount of dosage and (d) contact time on the AM dye adsorption on PLS.

stirring speed, which improves the interaction between PLS and the AM dye molecule and reduces the diffusion layer formed around the PLS. As a result, additional tests were conducted at the optimized stirring speed of 250 rpm.

3.5. Impact of PLS amount

To ensure cost-effectiveness, it's essential to determine the best amount of adsorbent to use. The impact of different amounts on the efficiency of removing AM dye was investigated by altering the quantity of sorbent from 10 to 80 mg/30 mL, as shown in Figure 6c. The results indicate a rapid increase in dye removal efficiency, from 23 ± 1.331 to $91.5 \pm 1.611\%$, as the mass of PLS increased from 10 to 50 mg. This increase is due to the greater surface area and active sites provided by the higher amount of PLS. However, increasing the PLS amount beyond 50 mg did not improve the removal efficiency since the maximal amount of dye was already adsorbed, and no more was available.[36] Therefore, 50 mg was determined to be the optimal PLS dosage for further experiments.

3.6. Influence of contact duration

Examining the duration of contact between the adsorbent and adsorbate is crucial throughout the sorption process. For example, the adsorption of AM dye by PLS was investigated at varied starting dye concentrations (20, 80, 140, and 200 mg/L) and at different time durations (from 0 to 240 min). The outcomes demonstrated how quickly the dye was removed in the early going (Figure 6d). But when it got closer to balance, it slowed down a bit. This is a result of the fact that free surface areas were accessible during the first adsorption phase. The adsorbate on the adsorbent surface and in the bulk phase would experience a repulsive force when dye molecules eventually filled the empty spaces. After stirring the adsorbent-containing solutions for up to 60 min, equilibrium is reached. After reaching equilibrium, there was no discernible change in the dye adsorption % over time. This implies that more treatment does not result in more significant elimination once equilibrium is reached. The movement of dye molecules from the exterior to the interior sites of the biosorbent particles governs the pace at which the adsorbate is removed from water solutions in

batch adsorption.[37] Therefore, based on the results, the equilibrium time was taken as 60 min for further testing.

3.7. Adsorption kinetics

The study of kinetics is essential in assessing adsorption. It helps determine the appropriate contact time to control the process and identify the primary adsorption mechanism. To evaluate the adsorption of AM by PLS, the equilibrium data has been fitted into well-established pseudo-first-order (PFO) and pseudo-second-order (PSO) kinetic models. This enables an accurate assessment of the kinetics of the process. The PFO and PSO non-linear models are derived employing Equation (4) and Equation (5), as follows:

$$q_t = q_e(1 - e^{-k_1 t}) \tag{4}$$

$$q_t = \frac{q_e^2 k_2 t}{1 + q_e k_2 t} \tag{5}$$

Here, q_t and q_e represent the quantities of AM sorbed at equilibrium and at time t, respectively. k_1 and k_2 are the rate constants for PFO and PSO, respectively. Figure 7 shows the fitted curves of AM dye, while Table 2 lists the rate constants, regression coefficients (R^2), and other variables calculated by the two models. The higher R^2 values confirmed that the PSO is the best-fitted kinetic model for AM

adsorption onto PLS than the PFO model for all concentrations. The kinetic study describes that AM adsorption onto PLS follows chemisorption mechanisms. However, the experimental q_e values for AM adsorption were closer to the theoretically calculated q_e values of the PFO model. It indicated the occurrence of the physisorption (electrostatic interaction) mechanism for AM adsorption onto PLS.

The model of intraparticle diffusion (IPD) introduced by Weber and Morris elucidates how the transfer of AM occurs from the aqueous solution to the adsorption sites of PLS. According to this model, the overall rate of adsorption is governed by the type of physical or chemical bond established between the solute and the solid at specific locations within the solid. The linearized IPD model is given as Equation (6):

$$q_t = k_{id} t^{0.5} + C \tag{6}$$

where k_{id} (mg/g min$^{0.5}$) is the IPD rate constant, and the C (mg/g) value signifies a constant that illustrates the resistance to mass transfer within the boundary layer.

A plot of q_t against $t^{0.5}$ describes the IPD model with a k_{id} and C obtained as slope and intercept at different concentrations, respectively. The parameters concerning the IPD model are presented in Table 3, and the IPD rate constants for all plots follow the order of $k_{id,1} > k_{id,2} > k_{id,3}$. The steep slope observed for $k_{id,1}$ signifies the rapid adsorption
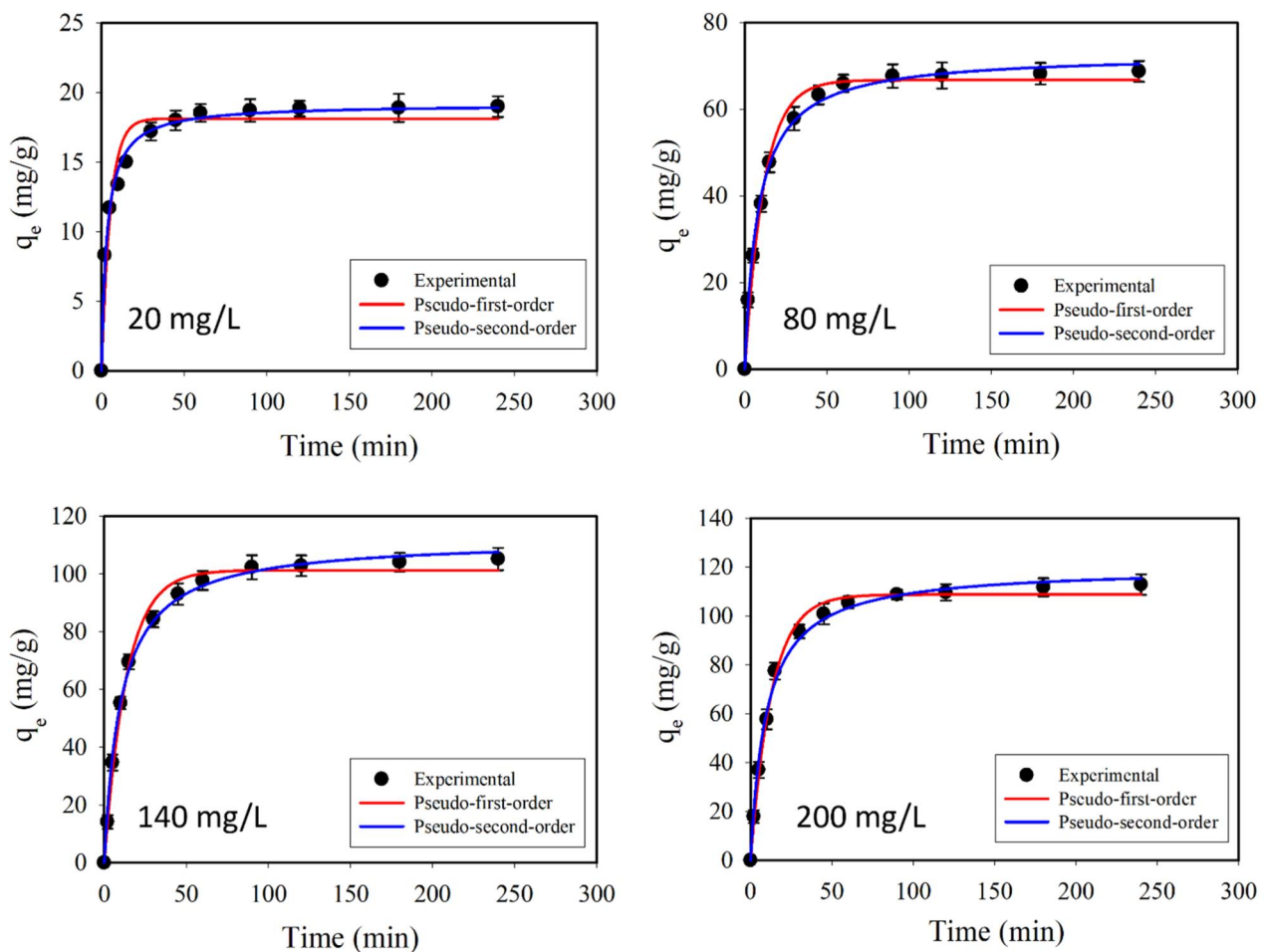

Figure 7. Kinetic plots of AM dye adsorption onto PLS at different concentrations.

Table 2. Adsorption kinetic model parameters for AM adsorption onto PLS at different concentrations.

Kinetic model	Parameters	Concentration of AM solution (mg/L)			
		20	80	140	200
Experimental value	qe, exp (mg/g)	18.5 ± 0.586	65.9 ± 1.006	102.3 ± 1.4115	105.6 ± 1.347
Pseudo-first-order	qe1, cal (mg/g)	18.12 ± 0.501	66.74 ± 1.048	101.34 ± 1.4057	108.7 ± 1.262
	k1 (1/min)	0.1877 ± 0.028	0.0872 ± 0.006	0.0743 ± 0.004	0.0773 ± 0.004
	R2	0.9497	0.9895	0.9911	0.9901
Pseudo-second-order	qe2, cal (mg/g)	19.16 ± 0.245	72.82 ± 0.811	112.19 ± 1.328	120.01 ± 1.703
	k2 (g/mg min)	0.0160 ± 0.0015	0.0017 ± 0.0001	0.0009 ± 0.00005	0.0009 ± 0.00006
	R2	0.9939	0.9985	0.9968	0.9972

Table 3. Intra-particle diffusion process for AM dye adsorption onto PLS.

| AM dye (mg/L)	First stage			Second state			Third stage		
	$k_{id,1}$ (mg/g min$^{0.5}$)	C_1 (mg/g)	R^2	$k_{id,2}$ (mg/g min$^{0.5}$)	C_2 (mg/g)	R^2	$k_{id,3}$ (mg/g min$^{0.5}$)	C_3 (mg/g)	R^2
20	2.619 ± 0.351	5.09 ± 0.99	0.9653	0.586 ± 0.039	14.01 ± 0.26	0.9955	0.043 ± 0.0086	18.32 ± 0.11	0.9243
80	12.934 ± 0.153	2.53 ± 0.43	0.9997	3.599 ± 0.534	38.45 ± 3.58	0.9785	0.179 ± 0.0242	65.90 ± 0.31	0.9645
140	22.527 ± 0.728	16.75 ± 2.06	0.9979	5.952 ± 0.747	52.16 ± 5.01	0.9845	0.485 ± 0.027	97.64 ± 0.34	0.9936
200	23.961 ± 0.769	16.51 ± 2.18	0.9979	5.267 ± 0.361	64.98 ± 2.42	0.9953	0.699 ± 0.047	102.05 ± 0.59	0.9911
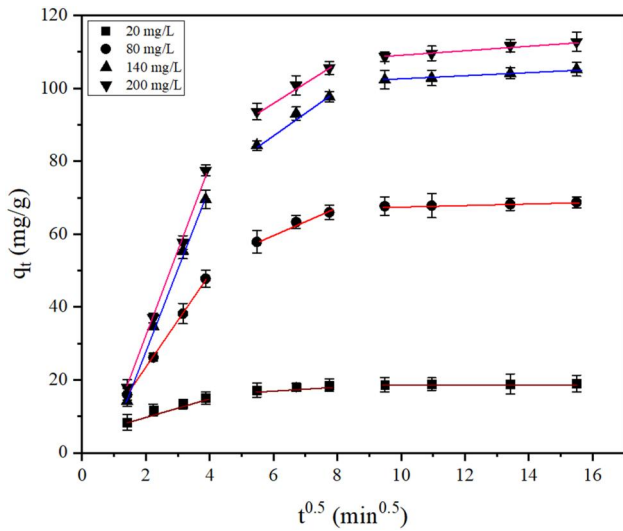
Figure 8. Intra-particle diffusion plots of AM dye adsorption onto PLS at different concentrations.

process of AM, attributed to the strong influence of bulk diffusion. The second slope, $k_{id,2}$, is more gradual, suggesting that AM molecules diffuse and adsorb into the pores at a slow rate. Finally, the third slope, $k_{id,3}$, appears nearly flat, suggesting the equilibrium saturation is reached at this stage.[38] The experimental data of all concentrations exhibit multi-linear plots (Figure 8), showing that the IPD is involved in the adsorption process. The linear plots do not pass through the origin, implying that IPD is not the only controlling step for the rate. Simultaneously, exterior mass transfer is also taking place, suggesting that both external mass transfer and IPD may jointly control the overall adsorption process.[39]

3.8. Modeling of adsorption isotherms

The isotherm models are essential for calculating sorption capacity, optimizing adsorbent consumption, and building a suitable sorption system. These models show the interaction of the sorbent and dye. To further understand the sorption mechanism and the interaction of the dye with PLS, an isotherm analysis was carried out using three models: Freundlich, Langmuir, and Temkin.

The Langmuir model is an assumption that the sorption process takes place on a solid surface, where the surface has homogeneous sites that are identical. According to this model, the adsorption of dye molecules stops once all the active sites are covered. The Langmuir isotherm is represented by Equation (7):

$$q_e = \frac{q_{max} K_L C_e}{1 + K_L C_e} \qquad (7)$$

where C_e (mg/L) is the equilibrium concentration of the AM in the solution, q_e (mg/g) the equilibrium sorption, q_{max} (mg/g) the sorption uptake (i.e., maximum equilibrium sorption) of the PLS, and K_L (L/mg) the Langmuir model constant, which is related to the energy of sorption.

The Freundlich isotherm assumes a non-uniform thermal distribution on the sorbent surface, representing heterogeneous adsorption. It can be expressed by Equation (8):

$$q_e = K_f C_e^{1/n} \qquad (8)$$

where n and K_F (mg/g) are empirical constants of the Freundlich model. $1/n$ represents the adsorption intensity, and K_F the relative adsorption uptake. The value of 'n' ranging from 1.0 to 10 indicated that the sorption process is favorable. The 'n' values of PLS for AM adsorption were >1 at all concentrations (Table 4), suggesting that it could be considered a favorable adsorption system.

The Temkin isotherm includes a factor that specifically considers the interactions between the adsorbent and adsorbate. This equation assumes that due to these interactions, and by disregarding very low and very high concentration values, the adsorption heat of all molecules in the layer decreases linearly as coverage rises. The Temkin isotherm is expressed by Equation (9):

$$q_e = \frac{RT}{B_T} \; ln(A_T C_e) \qquad (9)$$

where q_e (mg/g) is the quantity of adsorbate adsorbed at equilibrium, A_T (L/g) is the equilibrium binding constant, R is the gas constant, C_e (mg/L) is the final concentration of

Table 4. Adsorption isotherm parameters for AM adsorption onto PLS at different temperatures.

Isotherm model	Parameters	Temperature (K)			
		298	308	318	328
Langmuir	q_{max} (mg/g)	121.3 ± 1.493	116.23 ± 2.676	105.9 ± 2.499	101 ± 2.587
	K_L (L/mg)	0.1001 ± 0.004	0.0924 ± 0.007	0.0883 ± 0.007	0.0708 ± 0.006
	R^2	0.9991	0.9965	0.9961	0.9958
Freundlich	K_f (mg/g)	26.5 ± 4.273	24.9 ± 4.783	22.9 ± 4.461	19.4 ± 3.962
	n	3.023 ± 0.0404	3.043 ± 0.479	3.103 ± 0.495	2.952 ± 0.457
	R^2	0.9521	0.9348	0.9360	0.9405
Temkin	B_T (J/mol)	24.44 ± 1.034	23.28 ± 1.454	21.91 ± 1.424	21.47 ± 1.412
	A_T (L/g)	1.204 ± 0.142	1.064 ± 0.202	0.943 ± 0.179	0.708 ± 0.124
	R^2	0.9927	0.9916	0.9937	0.9911
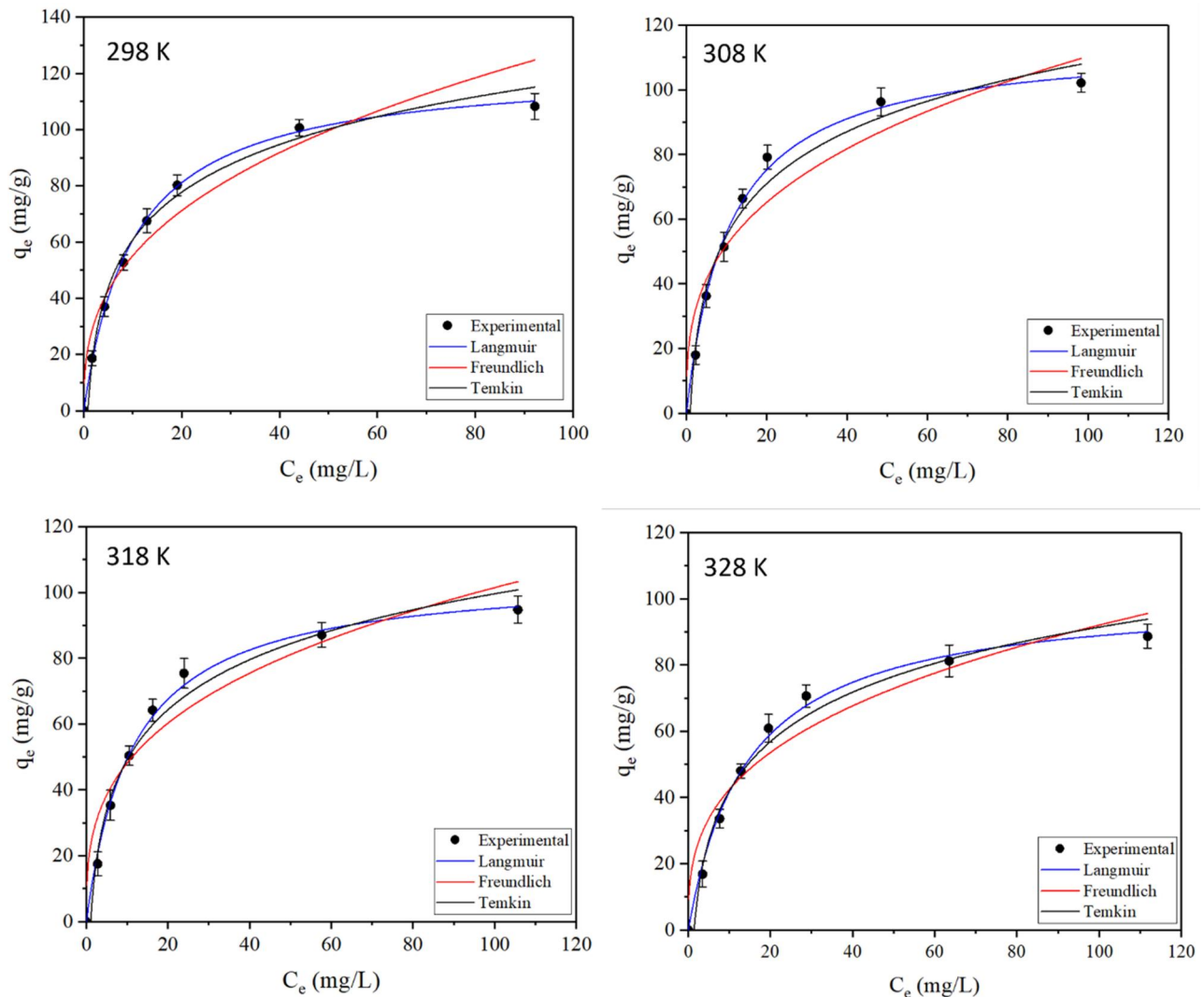
Figure 9. Isotherm plots of AM dye adsorption onto PLS at different temperatures.

adsorbate, B_T (J/mol) is the constant related to the heat capacity, and T is the temperature.

The models of Freundlich, Langmuir, and Temkin isotherms that were used to match the experimental data at several temperatures are shown in Figure 9. Table 4 shows the constant parameters and regression coefficients for the isotherm models. With the greatest R^2 value and the best match across all temperatures, the Langmuir isotherm demonstrated the homogeneous PLS surface and monolayer sorption coverage. The maximum adsorption uptake dropped from 121.3 ± 1.493 to 101 ± 2.587 mg/g as the

Table 5. Comparison of the adsorption uptake of AM onto PLS with various adsorbents.

| Adsorbent	Uptake mg/g	pH	Reference
$WS_2/Fe_3O_4/CNTs-NC$	174.8	3.0	[3]
Peltophorum pterocarpum leaf	133.33	2.0	[42]
Papaya leaf stalks (PLS)	121.3 ± 1.493	2.0	Present study
Terminalia chebula shell	102.4	2.0	[42]
Aminated avocado seed powder	89.2	2.0	[33]
$Fe_3O_4@nSiO_2@mSiO_2@DHIM-NH_2$	84.4	2.0	[43]
$Fe_3O_4@mZrO_2/rGO$	76.9	2.0	[34]
ZnO nanoparticles	75.9	7.0	[44]
Water hyacinth leaves	70.61	–	[4]
CS-PEI-GLA	48.3	5.0	[45]
Fe_3O_4/MgO nanoparticles	38.1	9.0	[6]
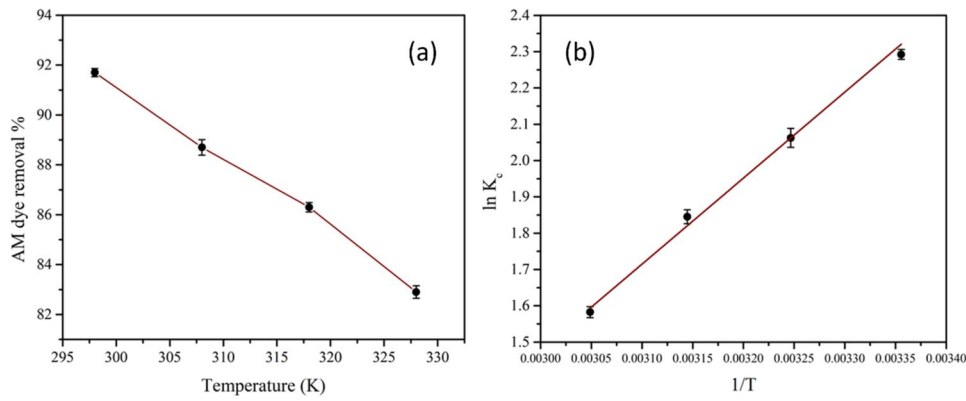
Figure 10. (a) Effect of temperature on the removal of AM by PLS and (b) Van't Hoff plot.

temperature rose from 298 to 328 K, demonstrating the exothermic character of the sorption. The exothermic character of the AM sorption process was further supported by the fact that the values of K_f in the Freundlich isotherm model dropped as the temperature climbed.[40] Furthermore, when the temperature rose, the Langmuir constant K_L dropped, suggesting that the PLS may have a higher affinity $(0.1001 \pm 0.004 \, \text{L/mg})$ for AM dye molecules at lower temperatures.[41]

3.9. Comparison of PLS with other adsorbents for AM dye

Several studies have been conducted on the adsorption of AM dye on various substrates. Table 5 displays the most notable adsorption effectiveness of dye AM on different adsorbents.[3,4,6,33,34,42–45] The equilibrium adsorption yield indicates that the value assessed in this study is reasonable compared to other materials. This is due to the high specific surface area and number of active sites. It has been determined that PLS can be utilized as a dye-removal adsorbent.

3.10. Effect of solution temperature and thermodynamic study

The adsorption of AM on PLS is affected by temperature, which determines if the reaction is spontaneous and if the adsorption mechanism is physical or chemical. To understand the temperature effect on this process, the researchers studied the adsorption of AM on PLS between 298 to 323 K. The outcomes indicated that as the temperature rose from 298 to 323 K, the dye removal efficiency decreased from $91.7 \pm 0.162\%$ to $82.9 \pm 0.258\%$ (Figure 10a). This could be due to either damage to the biosorbent's dynamic binding destinations or the growing dye's tendency to desorb from an interface near the solution. These observations suggest that the adsorption of AM on the PLS is an exothermic process.[46] Based on these findings, the optimum temperature for this process was determined to be 298 K.

To better understand the adsorption process, we can study its thermodynamic mechanism by considering temperature as a key factor. The thermodynamic parameters that can help us do this are the change in Gibbs free energy

Table 6. Adsorption thermodynamic parameters for AM adsorption onto PLS.

Temperature (K)	ΔG^o (kJ/mol)	ΔS^o (J/mol K)	ΔH^o (kJ/mol)
298	-5.5555 ± 0.038		
308	-5.28127 ± 0.042	-41 ± 0.057	-17.8 ± 0.093
318	-4.87828 ± 0.046		
328	-4.31541 ± 0.029		

(ΔG^o), enthalpy (ΔH^o), and entropy (ΔS^o). We can calculate these parameters using the following Eqs.:

$$\ln K_c = -[\Delta H^o / RT] + [\Delta S^o / R] \tag{10}$$

$$K_c = \frac{C_o - C_e}{C_e} \tag{11}$$

$$\Delta G^o = -RT \ln K_c \tag{12}$$

$$\Delta G^o = \Delta H^o - T\Delta S^o \tag{13}$$

$$\Delta S^o = \frac{\Delta H^o - \Delta G^o}{T} \tag{14}$$

Here, T is the temperature (Kelvin), R is the gas constant, and K_c is the distribution coefficient obtained by Equation (11). By plotting the Van't Hoff diagram, $\ln K_c$ vs. of $1/T$ (Figure 10b) and obtaining the line equation, the values of ΔH^o and ΔS^o could be extracted using slope and intercept, respectively. ΔG^o could be calculated employing Equation (12) at the desired temperatures. The thermodynamic variables were extracted at different temperatures and the results are tabulated in Table 6. The efficiency of removing AM was found to decline with increasing temperature. The small negative value of the ΔH^o (-17.8 ± 0.093 kJ/mol) suggests that the adsorption is physical and involves weak forces and attractive forces. It is also exothermic, indicating that the process is energetically stable. Additionally, the low ΔH^o value implies loose bonding between the adsorbate molecules and the sorbent surface.[47] The value of ΔS^o (-41 ± 0.057 J/mol K) suggests that the randomness decreases with the adsorption of AM at the interface of solid/solution. This indicates a lower degree of disorder at the PLS interface. Negative ΔG^o values indicate the spontaneity of the AM sorption process at different temperatures, with the adsorption of AM being highly affected by the solution temperature. The ΔG^o values increase as the temperature
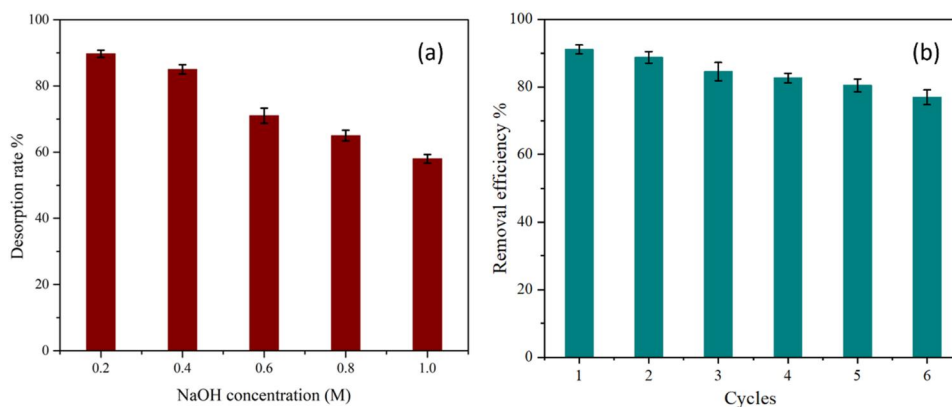
Figure 11. (a) Desorption performance at different NaOH concentrations and (b) Regeneration of PLS using 0.2 M NaOH.
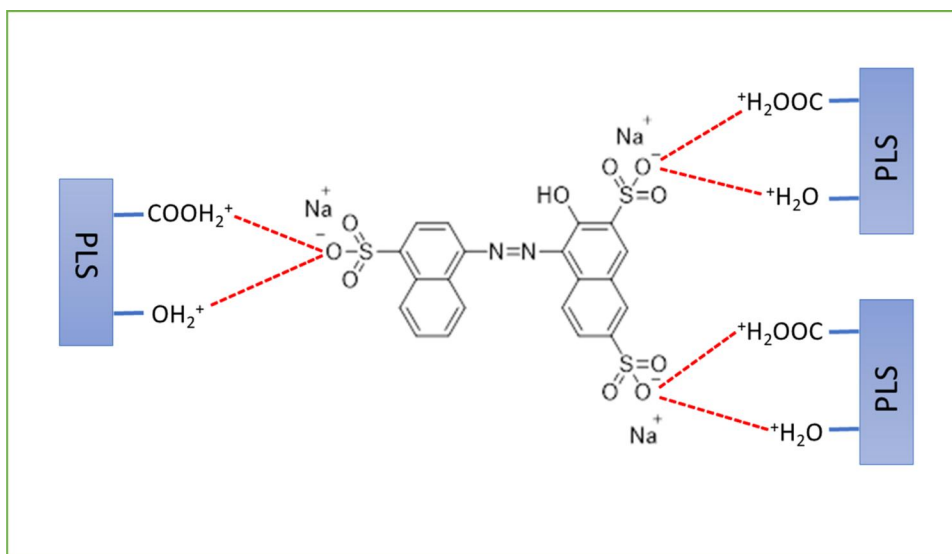

Figure 12. Possible interaction mechanism of AM with PLS.

increases, further illustrating the favorable adsorption process at lower temperatures.[48] Generally, $\Delta G°$ values range from 0 to -20 kJ/mol for physisorption and -80 to -400 kJ/mol for chemisorption.[49] In this study, the $\Delta G°$ values vary between -5.5555 ± 0.038 and -4.31541 ± 0.029 kJ/mol, which indicates that the AM sorption reaction can be physisorption.

3.11. Desorption and regeneration of the PLS

Desorption and reusability studies of an adsorbent are crucial for understanding the mechanisms of solute transfer, enhancing process economics, and determining its practical utility and potential for commercial-scale applications. The desorption of the adsorbed AM from PLS was explored at different concentrations of NaOH, and the results are shown in Figure 11a. Based on the findings of the study, it was observed that the desorption efficiency was reduced with a rise in NaOH concentrations. The reduction in dye desorption at higher eluent concentrations was attributed to the degradation of active sites on the biosorbent's surface.[50] The maximal desorption efficiency of $89.2 \pm 1.184\%$ was

achieved with 0.2 M NaOH solution. Furthermore, the reusability tests were conducted for up to six cycles, and the regenerated PLS's removal efficiencies for AM were calculated. The removal efficiency of the PLS gradually reduced as the number of regeneration cycles increased. This trend was attributed to reduced surface properties and functional groups on the adsorbent surface, which decreased active adsorption sites. Nonetheless, the outcomes depicted in Figure 11b reveal that the sorbent maintained an efficiency of $> 75\%$ even after six use cycles. This indicated that PLS could be employed as a reusable sorbent for treating wastewater containing anionic dyes.

3.12. Possible mechanism of adsorption

In an aqueous solution, the anionic dye Amaranth (AM) dissociates into AM-SO_3^-. Meanwhile, PLS is a cellulosic material that contains a majority of -OH and -COOH groups, which has been confirmed by FTIR (Figure 1). Based on the structure of the AM, the surface property of the PLS and the experimental results, the mechanism involved during dye adsorption can be described as follows:

- The AM dye molecules move from the solution to the surface of the PLS.
- The dye diffuses toward the surface of the biosorbent through a boundary layer and
- The dye is adsorbed on the surface of the biosorbent due to electrostatic interaction, as depicted in Figure 12.

4. Conclusions

In the present study, papaya leaf stalks (PLS) were used as the adsorbent material. The prepared PLS was characterized by FTIR, SEM, XRD, BET/BJH, and EDX analysis. These results confirmed that the prepared PLS has sufficient characteristics, including porous, roughness, surface area, pore volume, necessary functional groups, and required elemental composition, for the AM dye removal from contaminated water. The PLS dose, pH, contact duration, temperature, agitation speed, and initial dye concentration all substantially impacted AM adsorption. Under the optimum conditions, the maximal removal efficiency ($R\%$) and adsorption uptake (q_{max}) for AM due were found to be $91.1 \pm 2.601\%$ and 121.3 ± 1.493 mg/g, respectively. The comparison of the sorption uptake (q_{max}) of PLS with various other biosorbents depicted in previous literature for the elimination of AM is listed in Table 5. The kinetics of the sorption process were characterized by a rapid starting stage occurring within the first 60 min. The kinetic studies showed that AM dye on PLS was well fitted by PSO ($R^2 > 0.9939$), indicating that the adsorption kinetics was jointly controlled by exterior mass transfer and IPD. The equilibrium sorption data for AM adsorption onto PLS aligned well with the Langmuir model ($R^2 > 0.9958$). The thermodynamic variables associated with AM adsorption were studied at different temperatures, and the Van't Hoff model was utilized to illustrate the adsorption process's feasibility, spontaneity, and exothermic nature. The maximal AM desorption ($89.2 \pm 1.184\%$) from PLS was achieved using 0.2 M NaOH. After six cycles, the removal efficiency of AM dye reached $76.9 \pm 2.204\%$, showing a good reusability of PLS performance. The sorption mechanisms of AM onto PLS were also thoroughly explored. The adsorption process involved dominant physisorption together with necessary chemisorption. In more detail, the sorption mechanism involved pore filling and electrostatic interactions. Based on these results, this study concluded that PLS is a low-cost adsorbent with more significant potential for removing AM dye from contaminated water.

Disclosure statement

No potential conflict of interest was reported by the author(s).

Funding

References

[1] Qais, D. S.; Islam, M. N.; Othman, M. H. D.; Mahmud, H. N. M. E.; Quayum, M. E.; Islam, M. A.; Ismail, I. M. I.; Habib, A. Nano-Zinc Oxide Fibers: Synthesis, Characterization, Adsorption of Acid Blue 92 Dye, Isotherms, Thermodynamics and Kinetics. *Emerg. Contam.* **2023**, *9*, 100224. DOI: 10.1016/j.emcon.2023.100224.

[2] Wang, F.; Li, L.; Iqbal, J.; Yang, Z.; Du, Y. Preparation of Magnetic Chitosan Corn Straw Biochar and Its Application in Adsorption of Amaranth Dye in Aqueous Solution. *Int. J. Biol. Macromol.* **2022**, *199*, 234–242. DOI: 10.1016/j.ijbiomac.2021.12.195.

[3] Arabkhani, P.; Javadian, H.; Asfaram, A.; Sadeghfar, F.; Sadegh, F. Synthesis of Magnetic Tungsten Disulfide/Carbon Nanotubes Nanocomposite (WS_2/Fe_3O_4/CNTs-NC) for Highly Efficient Ultrasound-Assisted Rapid Removal of Amaranth and Brilliant Blue FCF Hazardous Dyes. *J. Hazard Mater.* **2021**, *420*, 126644. DOI: 10.1016/j.jhazmat.2021.126644.

[4] Guerrero-Coronilla, I.; Morales-Barrera, L.; Cristiani-Urbina, E. Kinetic, Isotherm and Thermodynamic Studies of Amaranth Dye Biosorption from Aqueous Solution onto Water Hyacinth Leaves. *J. Environ. Manage* **2015**, *152*, 99–108. DOI: 10.1016/j.jenvman.2015.01.026.

[5] Anjaneya, O.; Shrishailnath, S. S.; Guruprasad, K.; Nayak, A. S.; Mashetty, S. B.; Karegoudar, T. B. Decolourization of Amaranth Dye by Bacterial Biofilm in Batch and Continuous Packed Bed Bioreactor. *Int. Biodeterior. Biodegrad.* **2013**, *79*, 64–72. DOI: 10.1016/j.ibiod.2013.01.006.

[6] Salem, A. N. M.; Ahmed, M. A.; El-Shahat, M. F. Selective Adsorption of Amaranth Dye on Fe_3O_4/MgO Nanoparticles. *J. Mol. Liq.* **2016**, *219*, 780–788. DOI: 10.1016/j.molliq.2016.03.084.

[7] Khan, Z. A.; Elwakeel, K. Z.; Mashabi, R. A.; Elgarahy, A. M. Adsorption of Anionic Dyes onto 1,5-Diphenylcarbazide Functionalized Magnetic Hybrid Polymer: Impact of Water Salinity and Surfactants on Adsorption Isotherms. *J. Ind. Eng. Chem.* **2024**, *131*, 569–584. DOI: 10.1016/j.jiec.2023.10.061.

[8] Watwe, V.; Kulkarni, S.; Kulkarni, P. Development of Dried Uncharred Leaves of Ficus Benjamina as a Novel Adsorbent for Cationic Dyes: Kinetics, Isotherm, and Batch Optimization. *Ind. Crops Prod.* **2023**, *195*, 116449. DOI: 10.1016/j.indcrop.2023.116449.

[9] Munagapati, V. S.; Yarramuthi, V.; Kim, Y.; Lee, K. M.; Kim, D. S. Removal of Anionic Dyes (Reactive Black 5 and Congo Red) from Aqueous Solutions Using Banana Peel Powder as an Adsorbent. *Ecotoxicol. Environ. Saf.* **2018**, *148*, 601–607. DOI: 10.1016/j.ecoenv.2017.10.075.

[10] Prasad, K. S. N. V.; Veluru, S.; Himaja Pamu, S.; Rao Poiba, V.; Talib Hamzah, H.; Seereeddi, M. Potential Efficacy of a Fruit Waste—Manila Tamarind Seed Powder for the Adsorption of Hazardous Dyes from Aqueous Solution: Batch Studies. *Mater. Today Proc.* **2023**, *80*, 1334–1340. DOI: 10.1016/j.matpr.2023.01.082.

[11] Rani, S.; Chaudhary, S. Adsorption of Methylene Blue and Crystal Violet Dye from Waste Water Using Citrus Limetta Peel as an Adsorbent. *Mater. Today Proc.* **2022**, *60*, 336–344. DOI: 10.1016/j.matpr.2022.01.237.

[12] Nipa, S. T.; Shefa, N. R.; Parvin, S.; Khatun, M. A.; Alam, M. J.; Chowdhury, S.; Khan, M. A. R.; Shawon, S. M. A. Z.; Biswas, B. K.; Rahman, M. W. Adsorption of Methylene Blue on Papaya Bark Fiber: Equilibrium, Isotherm and Kinetic Perspectives. *Results Eng.* **2023**, *17*, 100857. DOI: 10.1016/j.rineng.2022.100857.

[13] Zhang, Z.; O'Hara, I. M.; Kent, G. A.; Doherty, W. O. S. Comparative Study on Adsorption of Two Cationic Dyes by Milled Sugarcane Bagasse. *Ind. Crops Prod.* **2013**, *42*, 41–49. DOI: 10.1016/j.indcrop.2012.05.008.

[14] Yadav, K.; Latelwar, S. R.; Datta, D.; Jana, B. Efficient Removal of MB Dye Using Litchi Leaves Powder Adsorbent: Isotherm

and Kinetic Studies. *J. Indian Chem. Soc.* **2023**, *100*, 100974. DOI: 10.1016/j.jics.2023.100974.

[15] Fathi, M. R.; Asfaram, A.; Farhangi, A. Removal of Direct Red 23 from Aqueous Solution Using Corn Stalks: Isotherms, Kinetics and Thermodynamic Studies. *Spectrochim. Acta A Mol. Biomol. Spectrosc.* **2015**, *135*, 364–372. DOI: 10.1016/j.saa.2014.07.008.

[16] Asif Tahir, M.; Bhatti, H. N.; Iqbal, M. Solar Red and Brittle Blue Direct Dyes Adsorption onto Eucalyptus Angophoroides Bark: Equilibrium, Kinetics and Thermodynamic Studies. *J. Environ. Chem. Eng.* **2016**, *4*, 2431–2439. DOI: 10.1016/j.jece.2016.04.020.

[17] Bazzo, A.; Adebayo, M. A.; Dias, S. L. P.; Lima, E. C.; Vaghetti, J. C. P.; de Oliveira, E. R.; Leite, A. J. B.; Pavan, F. A. Avocado Seed Powder: Characterization and Its Application for Crystal Violet Dye Removal from Aqueous Solutions. *Desalin. Water Treat* **2016**, *57*, 15873–15888. DOI: 10.1080/19443994.2015.1074621.

[18] Karim, A. R.; Danish, M.; Alam, M. G.; Majeed, S.; Alanazi, A. M. A Review of Pre- and Post-Surface-Modified Neem (Azadirachta Indica) Biomass Adsorbent: Surface Functionalization Mechanism and Application. *Chemosphere* **2024**, *351*, 141180. DOI: 10.1016/j.chemosphere.2024.141180.

[19] Rose, P. K.; Kumar, R.; Kumar, R.; Kumar, M.; Sharma, P. Congo Red Dye Adsorption onto Cationic Amino-Modified Walnut Shell: Characterization, RSM Optimization, Isotherms, Kinetics, and Mechanism Studies. *Groundw. Sustain. Dev.* **2023**, *21*, 100931. DOI: 10.1016/j.gsd.2023.100931.

[20] Ghosh, I.; Kar, S.; Chatterjee, T.; Bar, N.; Das, S. K. Removal of Methylene Blue from Aqueous Solution Using Lathyrus Sativus Husk: Adsorption Study, MPR and ANN Modelling. *Process Saf. Environ. Prot.* **2021**, *149*, 345–361. DOI: 10.1016/j.psep.2020.11.003.

[21] Zaidi, N. A. H. M.; Lim, L. B. L.; Usman, A. Enhancing Adsorption of Malachite Green Dye Using Base-Modified Artocarpus Odoratissimus Leaves as Adsorbents. *Environ. Technol. Innov.* **2019**, *13*, 211–223. DOI: 10.1016/j.eti.2018.12.002.

[22] Debnath, S.; Ballav, N.; Maity, A.; Pillay, K. Competitive Adsorption of Ternary Dye Mixture Using Pine Cone Powder Modified with β-Cyclodextrin. *J. Mol. Liq.* **2017**, *225*, 679–688. DOI: 10.1016/j.molliq.2016.10.109.

[23] Georgin, J.; Dotto, G. L.; Mazutti, M. A.; Foletto, E. L. Preparation of Activated Carbon from Peanut Shell by Conventional Pyrolysis and Microwave Irradiation-Pyrolysis to Remove Organic Dyes from Aqueous Solutions. *J. Environ. Chem. Eng.* **2016**, *4*, 266–275. DOI: 10.1016/j.jece.2015.11.018.

[24] Sultana, S.; Islam, K.; Hasan, M. A.; Khan, H. M. J.; Khan, M. A. R.; Deb, A.; Al Raihan, M.; Rahman, M. W. Adsorption of Crystal Violet Dye by Coconut Husk Powder: Isotherm, Kinetics and Thermodynamics Perspectives. *Environ. Nanotechnol. Monit. Manag.* **2022**, *17*, 100651. DOI: 10.1016/j.enmm.2022.100651.

[25] Stavrinou, A.; Aggelopoulos, C. A.; Tsakiroglou, C. D. Exploring the Adsorption Mechanisms of Cationic and Anionic Dyes onto Agricultural Waste Peels of Banana, Cucumber and Potato: Adsorption Kinetics and Equilibrium Isotherms as a Tool. *J. Environ. Chem. Eng.* **2018**, *6*, 6958–6970. DOI: 10.1016/j.jece.2018.10.063.

[26] Mercy Jasper, P.; Sumithra, S.; Jameer Ahammad, S.; Madakka, M. Exploring Biosorption Properties of Litchi Chinensis Peel for a Cationic Dye Rhodamine 6G in Liquid/Solid Phase System: Kinetics and Equilibrium Studies. *Watershed Ecol. Environ.* **2022**, *4*, 66–72. DOI: 10.1016/j.wsee.2022.08.001.

[27] Akdemir, M.; Isik, B.; Cakar, F.; Cankurtaran, O. Comparison of the Adsorption Efficiency of Cationic (Crystal Violet) and Anionic (Congo Red) Dyes on Valeriana Officinalis Roots: Isotherms, Kinetics, Thermodynamic Studies, and Error Functions. *Mater. Chem. Phys.* **2022**, *291*, 126763. DOI: 10.1016/j.matchemphys.2022.126763.

[28] Subbaiah Munagapati, V.; Wen, H. Y.; Gollakota, A. R. K.; Wen, J. C.; Andrew Lin, K. Y.; Shu, C. M.; Mallikarjuna Reddy, G.; Zyryanov, G. V.; Wen, J. H.; Tian, Z. Removal of Sulfonated Azo Reactive Red 195 Textile Dye from Liquid Phase Using Surface-Modified Lychee (Litchi Chinensis) Peels with Quaternary Ammonium Groups: Adsorption Performance, Regeneration, and Mechanism. *J. Mol. Liq.* **2022**, *368*, 120657. DOI: 10.1016/j.molliq.2022.120657.

[29] Liang, S.; Guo, X.; Feng, N.; Tian, Q. Isotherms, Kinetics and Thermodynamic Studies of Adsorption of Cu^{2+} from Aqueous Solutions by Mg^{2+}/K^+ Type Orange Peel Adsorbents. *J. Hazard Mater.* **2010**, *174*, 756–762. DOI: 10.1016/j.jhazmat.2009.09.116.

[30] Gemici, B. T.; Ozel, H. U.; Ozel, H. B. Removal of Methylene Blue onto Forest Wastes: Adsorption Isotherms, Kinetics and Thermodynamic Analysis. *Environ. Technol. Innov.* **2021**, *22*, 101501. DOI: 10.1016/j.eti.2021.101501.

[31] Munagapati, V. S.; Kim, D. S. Adsorption of Anionic Azo Dye Congo Red from Aqueous Solution by Cationic Modified Orange Peel Powder. *J. Mol. Liq.* **2016**, *220*, 540–548. DOI: 10.1016/j.molliq.2016.04.119.

[32] Babalola, J. O.; Koiki, B. A.; Eniayewu, Y.; Salimonu, A.; Olowoyo, J. O.; Oninla, V. O.; Alabi, H. A.; Ofomaja, A. E.; Omorogie, M. O. Adsorption Efficacy of Cedrela Odorata Seed Waste for Dyes: Non Linear Fractal Kinetics and Non Linear Equilibrium Studies. *J. Environ. Chem. Eng.* **2016**, *4*, 3527–3536. DOI: 10.1016/j.jece.2016.07.027.

[33] Munagapati, V. S.; Wen, H. Y.; Vijaya, Y.; Wen, J. C.; Wen, J. H.; Tian, Z.; Reddy, G. M.; Raul Garcia, J. Removal of Anionic (Acid Yellow 17 and Amaranth) Dyes Using Aminated Avocado (Persea Americana) Seed Powder: Adsorption/ Desorption, Kinetics, Isotherms, Thermodynamics, and Recycling Studies. *Int. J. Phytoremediation* **2021**, *23*, 911–923. DOI: 10.1080/15226514.2020.1866491.

[34] Jiang, H.; Chen, P.; Zhang, W.; Luo, S.; Luo, X.; Au, C.; Li, M. Deposition of Nano Fe_3O_4 @mZrO_2 onto Exfoliated Graphite Oxide Sheets and Its Application for Removal of Amaranth. *Appl. Surf. Sci.* **2014**, *317*, 1080–1089. DOI: 10.1016/j.apsusc.2014.09.023.

[35] Hegde, V.; Uthappa, U. T.; Mane, P. V.; Ji, S. M.; Suneetha, M.; Wang, B.; Altalhi, T.; Subrahmanya, T. M.; Kurkuri, M. D. Design of Low-Cost Natural Casein Biopolymer Based Adsorbent for Efficient Adsorption of Multiple Anionic Dyes and Diclofenac Sodium from Aqueous Solutions. *Chemosphere* **2024**, *353*, 141571. DOI: 10.1016/j.chemosphere.2024.141571.

[36] Bensalah, H.; Younssi, S. A.; Ouammou, M.; Gurlo, A.; Bekheet, M. F. Azo Dye Adsorption on an Industrial Waste-Transformed Hydroxyapatite Adsorbent: Kinetics, Isotherms, Mechanism and Regeneration Studies. *J. Environ. Chem. Eng.* **2020**, *8*, 103807. DOI: 10.1016/j.jece.2020.103807.

[37] Banerjee, S.; Chattopadhyaya, M. C. Adsorption Characteristics for the Removal of a Toxic Dye, Tartrazine from Aqueous Solutions by a Low Cost Agricultural by-Product. *Arab. J. Chem.* **2017**, *10*, S1629–S1638. DOI: 10.1016/j.arabjc.2013.06.005.

[38] Malik, S. A.; Dar, A. A.; Banday, J. A. Kinetic and Adsorption Isotherm Studies of Malachite Green Dye onto Surfactant-Tailored Alginate Hydrogel Beads: An Influence of Surfactant Hydrophobicity. *Int J Biol Macromol.* **2024**, *263*, 130318. DOI: 10.1016/j.ijbiomac.2024.130318.

[39] Tanhaei, B.; Ayati, A.; Iakovleva, E.; Sillanpää, M. Efficient Carbon Interlayed Magnetic Chitosan Adsorbent for Anionic Dye Removal: Synthesis, Characterization and Adsorption Study. *Int. J. Biol. Macromol.* **2020**, *164*, 3621–3631. DOI: 10.1016/j.ijbiomac.2020.08.207.

[40] Zhu, H.; Chen, S.; Duan, H.; He, J.; Luo, Y. Removal of Anionic and Cationic Dyes Using Porous Chitosan/Carboxymethyl cellulose-PEG Hydrogels: Optimization, Adsorption Kinetics, Isotherm and Thermodynamics Studies. *Int. J. Biol. Macromol.* **2023**, *231*, 123213. DOI: 10.1016/j.ijbiomac.2023.123213.

[41] Bayat, M.; Salehi, E.; Mahdieh, M. Chromochloris Zofingiensis Microalgae as a Potential Dye Adsorbent: Adsorption

Thermo-Kinetic, Isothermal, and Process Optimization. *Algal. Res.* **2023**, *71*, 103043. DOI: 10.1016/j.algal.2023.103043.

[42] Malleswari, P. V. N.; Swetha, S.; Jegadeesan, G. B.; Rangabhashiyam, S. Biosorption Study of Amaranth Dye Removal Using Terminalia Chebula Shell, Peltophorum Pterocarpum Leaf and Psidium Guajava Bark. *Int. J. Phytoremediation.* **2022**, *24*, 1081–1099. DOI: 10.1080/15226514.2021.2002261.

[43] Cheng, J.; Shi, L.; Lu, J. Amino Ionic Liquids-Modified Magnetic Core/Shell Nanocomposite as an Efficient Adsorbent for Dye Removal. *J. Ind. Eng. Chem.* **2016**, *36*, 206–214. DOI: 10.1016/j.jiec.2016.02.004.

[44] Zafar, M. N.; Dar, Q.; Nawaz, F.; Zafar, M. N.; Iqbal, M.; Nazar, M. F. Effective Adsorptive Removal of Azo Dyes over Spherical ZnO Nanoparticles. *J. Mater. Res. Technol.* **2019**, *8*, 713–725. DOI: 10.1016/j.jmrt.2018.06.002.

[45] Yusof, N. H.; Foo, K. Y.; Wilson, L. D.; Hameed, B. H.; Hussin, M. H.; Sabar, S. Microwave-Assisted Synthesis of Polyethyleneimine Grafted Chitosan Beads for the Adsorption of Acid Red 27. *J. Polym. Environ.* **2020**, *28*, 542–552. DOI: 10.1007/s10924-019-01628-3.

[46] Alabbad, E. A. Effect of Direct Yellow 50 Removal from an Aqueous Solution Using Nano Bentonite; Adsorption Isotherm, Kinetic Analysis and Also Thermodynamic Behavior. *Arab. J. Chem.* **2023**, *16*, 104517. DOI: 10.1016/j.arabjc.2022.104517.

[47] El-Bindary, A. A.; Hussien, M. A.; Diab, M. A.; Eessa, A. M. Adsorption of Acid Yellow 99 by Polycrylonitrile/Activated Carbon Composite: Kinetics, Thermodynamics and Isotherm Studies. *J. Mol. Liq.* **2014**, *197*, 236–242. DOI: 10.1016/j.molliq.2014.05.003.

[48] Lei, Y.; Yang, G.; Huang, Q.; Dou, J.; Dai, L.; Deng, F.; Liu, M.; Li, X.; Zhang, X.; Wei, Y. Facile Synthesis of Ionic Liquid Modified Silica Nanoparticles for Fast Removal of Anionic Organic Dyes with Extremely High Adsorption Capacity. *J. Mol. Liq.* **2022**, *347*, 117966. DOI: 10.1016/j.molliq.2021.117966.

[49] Adane, B.; Siraj, K.; Meka, N. Kinetic, Equilibrium and Thermodynamic Study of 2-Chlorophenol Adsorption onto Ricinus communis Pericarp Activated Carbon from Aqueous Solutions. *Green Chem. Lett. Rev.* **2015**, *8*, 1–12. DOI: 10.1080/17518253.2015.1065348.

[50] Maqbool, M.; Sadaf, S.; Bhatti, H. N.; Rehmat, S.; Kausar, A.; Alissa, S. A.; Iqbal, M. Sodium Alginate and Polypyrrole Composites with Algal Dead Biomass for the Adsorption of Congo Red Dye: Kinetics, Thermodynamics and Desorption Studies. *Surf. Interfaces* **2021**, *25*, 101183. DOI: 10.1016/j.surfin.2021.101183.